CHINESE JOURNAL OF PHYSICS VOL. 52, NO. 1-II February 2014

Review

Atomic and Molecular Photoelectron Holography in Strong Laser Fields

Xue-Bin Bian[1,2,*] and André D. Bandrauk[2]

[1]*State Key Laboratory of Magnetic Resonance and Atomic and Molecular Physics, Wuhan Institute of Physics and Mathematics, Chinese Academy of Sciences, Wuhan 430071, People's Republic of China*

[2]*Laboratoire de chimie théorique, Faculté des Sciences, Université de Sherbrooke, Québec, J1K2R1, Canada*

(Received August 29, 2013)

Recent progress in photoelectron holography with atoms and molecules in strong laser fields is reviewed. From a semi-classical model, four kinds of holography patterns are predicted, which include two forward rescattering interference patterns and two backward rescattering patterns involving subcycle interference of electron dynamics. One of the forward rescattering patterns has been experimentally demonstrated with mid-infrared free-electron lasers. The other three interference patterns are obtained from numerical simulations by solving the time-dependent Schrödinger equations for symmetric and nonsymmetric molecular ions in ultrashort intense lasers. It is shown that photoelectron holography is a new tool for attosecond-resolved imaging of molecular structure.

DOI: 10.6122/CJP.52.569 PACS numbers: 32.80.Wr, 33.60.+q, 61.05.jp

I. INTRODUCTION

The holographic method was first invented by Gabor [1] for improving the resolution limit of electron microscopy. The central idea is to use a *reference* wave to interfere with the *signal* wave to record both the amplitude and the phase information. The method is widely used in optics as the development of lasers. Photoelectron holography has been studied recently in new areas of research. It has been applied to image the crystal structure of solid surfaces [2]. Photoelectron holography in above-threshold ionization (ATI) from strong laser-atom and molecule interaction with elliptical and linear laser field has also been investigated [3–5]. In the process, part of free electrons after ionization directly arrive at a detector, while some of the free electrons are rescattered by the atomic or molecular cores, and then they reach the detector. We call the former as *reference* electrons and the latter as *signal* electrons, which contain detailed information on atomic and molecular structure. Photoelectron holography in ATI is unique and different from optical holography. The *reference* and *signal* photoelectrons produced by the strong laser field come from the same object, but with different transverse momentum. The *reference* and *signal* electrons with the same final momentum in the detector interfere with each other, thus recording

*Electronic address: xuebin.bian@wipm.ac.cn

both the phase and amplitude information of different trajectories. Photoelectrons with different final momentum correspond to different birth (ionization) times in the laser field, which can be determined approximately by a semiclassical model [4, 6, 7]. As a result, this kind of photoelectron holography is dynamic, and can be resolved on attosecond (1 as = 10^{-18} s) time scale, the scale of the electronic motion in matter [4, 7, 8]. The energy of the rescattered electron can reach up to 10 U_p [6], where $U_p = I/4m\omega^2$ is the ponderomotive energy at intensity I and frequency ω. The corresponding electron de Broglie wavelength $\lambda_e = 2\pi/p$ can be controlled and made comparable to or even smaller than molecular internuclear distances R, with Ångström (10^{-10} m) spatial resolution [9].

Since the *reference* and *signal* electrons register new information about the initial state and even atomic and molecular cores by laser-induced electron diffraction, LIED [10], photoelectron holography can be used as a new tool for dynamic imaging [10–12]. Photoelectron holography is a 4-D movie, recording the motion of electrons in molecules on their own attosecond time scale.

II. STRONG-FIELD MODEL FOR PHOTOELECTRON HOLOGRAPHY

In this section, we present photoelectron holography patterns in linearly polarized laser field obtained by a semiclassical model. The recollision model is described in the strong-field approximation (SFA) [6, 13, 14]. The following assumptions [7] form the basis of the model:

1. The phase changes during electron tunnel ionizaton and rescattering process are neglected. Multiple rescattering of the signal electron by the atomic and molecular cores is not considered.

2. Once the electrons are ionized, their motions are dominated by the laser field. The Coulomb force is neglected, the basis of the SFA model.

3. The initial velocity of the photoelectrons is zero after tunnelling ionization along the laser polarization direction. In the perpendicular direction, the initial velocity of the *reference* electrons is not zero, and is conserved. In this classical model, these electrons will not return to the cores due to their displacement in the perpendicular direction. For the *signal* electrons, their initial velocity in the perpendicular direction is zero. After ionization, when the laser field changes its phase (direction), some of the electrons will be driven back to the core and elastically rescattered to any direction.

4. We assume the free electrons are born at a distance $z_0 = I_p/E_0$ from the core by tunnelling ionization [15], where I_p is the ionization potential, E_0 is the amplitude of the laser field. This corresponds to ionization at the outer turning point of the potential barrier created by the Coulomb and static electric field E_0.

Assuming that the laser field is polarized along the z direction and the electric field is expressed by $E(t) = E_0 \cos(\omega t + \varphi)$, where ω is the carrier frequency and φ is the phase

where the electron is ionized, the velocity and the displacement of the free electron can be written from Newton's equations of motion $\ddot{z} = -E(t)$ (in atomic units: $e = \hbar = m = 1$) as:

$$\dot{z} = v(t,\phi) = \int_0^t -E(t')dt' = -\frac{E_0}{\omega}\left[\sin(\omega t + \phi) - \sin(\phi)\right], \tag{1}$$

$$z(t,\phi) = \int_0^t v(t')dt' = \frac{E_0}{\omega^2}\left[\cos(\omega t + \phi) - \cos(\phi) + \omega\sin(\phi)t\right] - z_0. \tag{2}$$

In this classical model, the signal electron is driven back to the parent core after a travel time t_c in the laser field, $z(t_c,\phi) = 0$. The relation between t_c and ϕ can be obtained from Eq. (1) and (2) ,

$$\cos(\omega t_c + \varphi) - \cos(\varphi) + \omega\sin(\varphi)t_c = \gamma^2/2, \tag{3}$$

where $\gamma = \frac{\omega}{E_0}\sqrt{2I_p}$ is the Keldysh parameter, the ratio of the bound electron energy to the free "dressed" or ponderomotive electron energy.

When the *signal* electron returns to the core, we assume it is elastically rescattered by the core at an angle θ_c . Then the velocity in the perpendicular direction is constant: $v_\perp = v(t_c,\phi)\sin(\theta_c)$. The velocity along the laser polarization direction is:

$$v_\parallel = \int_{t_c}^t E(t')dt' = -\frac{E_0}{\omega}\left[\sin(\omega t + \phi) - \sin(\omega t_c + \phi)\right] + v(t_c,\phi)\cos(\theta_c). \tag{4}$$

The total zero area condition, $\int E(t)dt = 0$, implies that the vector potential $A(t)$ is zero at the beginning and end of the pulse. From this condition, the measured final momentum by the detectors is:

$$P_\parallel = \frac{E_0}{\omega}\sin(\omega t_c + \phi) + v(t_c,\phi)\cos(\theta_c). \tag{5}$$

For the *reference* electrons, after setting their final momentum, the same as the *signal* electrons, one can calculate their ionization phase ϕ' and traveling time t^r. The phase difference between these two trajectories, *reference* and *signal*, is obtained as:

$$\Delta\Phi = \int_0^{t_c}\frac{v^2(t',\phi)}{2}dt' - \int_0^{t^r}\frac{v^2(t',\phi')}{2}dt' - \frac{v_\perp^2 t^r}{2} - I_p\frac{(\phi - \phi')}{\omega}. \tag{6}$$

In Figure 1, we show the typical interference patterns for *signal* and *reference* electrons ionized from different laser field quarter cycles. Fig. 1 (a) and (b) corresponds to total *forward* rescattering, while Fig. 1 (c) and (d) represents total *backward* rescattering. The interference dynamics are clearly occurring on subcycle time scale.

In ATI experiments, many interference patterns including temporal and spatial interference [16] will appear, such as ATI rings in a relatively long laser pulse [4, 7], time double-slit interference in phase-stabilized ultra short laser pulses [7, 17, 18]. How can

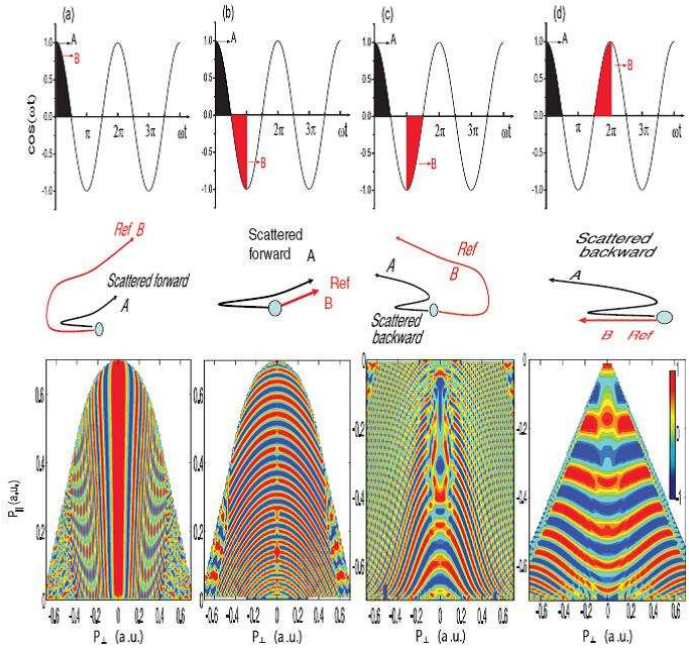

FIG. 1: Sketch of the interference trajectories from different subcycles in photoelectron holography. A represents the signal electron, B stands for the reference electron. The laser intensity is $I = 7.1 \times 10^{11}$ W/cm^2, and the wavelength is 7 μm. The ionization potential corresponds to the metastable $6s$ of Xe. Adapted from Ref. [7], copyright APS.

we separate the holography from the final spectra? To reduce the ATI rings and time double-slit interference patterns, one can change the length of the laser pulse to a medium length to observe clear holography patterns. In our numerical simulations, the total pulse duration between five and ten optical cycles is found to be optimal. To further disentangle the forward and backward rescattering holography patterns, one can choose atoms and molecules with relatively small and large rescattering cross sections to suppress or enhance the scattering probability.

III. PHOTOELECTRON HOLOGRAPHY WITH ATOMS IN STRONG LASER FIELD

As shown in Fig. 2, time-resolved atomic photoelectron holography was experimentally observed by Huismans *et al.* using a 7 μm free-electron laser (FEL) [4, 19]. This long wavelength FEL is favorable for the forward rescattering holography as illustrated in Fig. 1 (a). Due to the long period of this low-frequency laser field, the ionized electronic wave packets are widely spread when they are driven back to the core. As a result, the rescattering cross sections are relatively small, and the angular distributed forward rescattering holography pattern in Fig. 1 (a) calculated by SFA for Xe atom is clearly observed.

As described by our model in Section II, the Coulomb potential is neglected due to the dominant effect of the laser field. Taking into account Coulomb effects [4, 20], the experimental results and the results by solving the corresponding time-dependent Schrödinger equations (TDSE) agree well with the results by SFA, thus confirming the validity of SFA. The wide spreading of the wave packets is not helpful for observing the second forward rescattering holography pattern predicted by SFA as illustrated in Fig. 1 (b). The overlap of the two trajectories, *reference* and *signal*, is relatively small, as their amplitudes are not comparable.

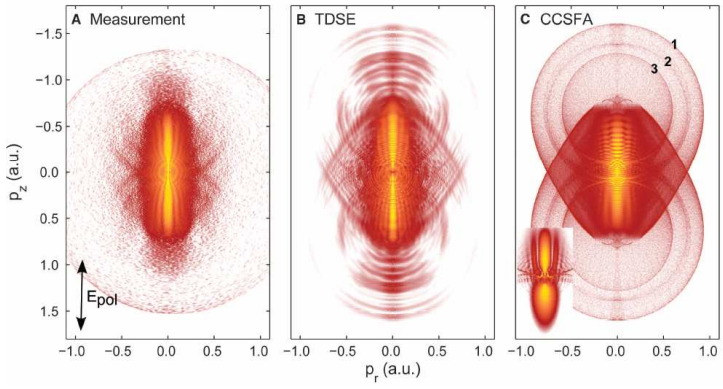

FIG. 2: Photoelectron momentum distribution of Xe 6*s* orbital in FEL. The laser parameters are the same as presented in Fig. 1. (a) is the experimental result. (b) is simulated by TDSE. (c) is obtained by Coulomb-corrected strong-field approximation. Adapted from Ref. [4], Copyright © 2011, American Association for the Advancement of Science.

The distribution of the *reference* electrons is essentially determined by the initial state of the system [7]. The photoelectron hologram will therefore image the initial wave function. It has been illustrated theoretically by using the degenerate $3s$, $3p$ and $3d$ states of the H as examples of an initial state, respectively [7]. The shape of the original orbital is imprinted in the photoelectron holography. It has also been experimentally confirmed that the shape and orientation of an initial Rydberg state leaves its own fingerprint on the final angular distribution of photoelectron spectra [21]. Thus photoelectron holography can provide an important new tool to extract useful orbital information by ultrafast strong-field processes.

In the SFA model described in Section II, multiple scattering of the signal electrons was neglected. Low-energy features in the spectra can reflect multiple rescattering of photoelectrons in laser fields [22–24]. The interference structure between unrescattered photoelectrons perpendicular to the laser polarization direction has also been confirmed experimentally and theoretically [25]. Such photoelectron spectra encode novel information of ultrafast processes in LIED.

The forward rescattering holographic patterns depend generally strongly on the laser wavelength λ and intensity I. It has been shown that the condition $U_p/\hbar\omega \gg 1$ is crucial for the holographic interference [26], i.e., high ponderomotive energy much larger than photon

energy. Although forward rescattering photoelectron holography has been clearly illustrated by using long-wavelength FELs [4], the backward rescattering photoelectron holography has not been identified yet experimentally.

IV. PHOTOELECTRON HOLOGRAPHY WITH MOLECULAR IONS IN STRONG LASER FIELD

To observe the backward rescattering holography, the scattering cross section must be relatively large as in molecules. In this section, we review the backward rescattering holography studied by using molecules with more scattering centres than atoms [8]. The wavelength of the laser field should be short to produce short recollision times, which are generally 2/3 of a laser cycle [7, 13, 14]. Short laser pulses also reduce the spread of the wavepackets. In addition, to reduce the dissociation effect of molecules in the ATI process, short-wavelength and short-pulse lasers in the near fs regime allow investigating the ultrafast process under Born-Oppenheimer approximation (BOA), corresponding to frozen nuclei. Coulomb focusing effect on the ionized electrons will also increase the relative scattering cross section [27]. Photoelectron holography from molecules should provide a useful tool for imaging molecular structure due to the above effects. We use symmetric H_2^+ [8] and asymmetric HeH^{2+} [28] molecular ions as examples to illustrate the motion of electrons in molecules measured by photoelectron holography.

In the simulations, the wavelength of the laser field used is $\lambda = 532$ nm (1 optical cycle is around 1.8 fs), the laser intensity is $I = 1.5 \times 10^{15}$ W/cm^2. The total pulse duration is $T = 5$ cycles with polarization along the z axis. The vector potential of the pulse is given by $A(t) = \frac{E_0}{\omega} \sin^2(\frac{\pi t}{T}) \cos(\omega t)$, thus ensuring total zero area for $E(t) = -\frac{\partial A(t)}{\partial t}$. The vibrational period of H_2^+ is around 15 fs. The total duration of the laser pulse is around 9 fs. The dominant ionization time of photoelectron occurs around two cycles near the peak intensity of the pulse. Furthermore the recollision time t_c is around 1 fs, thus making the fixed-nuclei approximation in the numerical simulations valid. We set the internuclear distance at equilibrium $R = 2$ a.u. The photoelectron angular momentum distribution of H_2^+ is illustrated in Fig. 3 with both parallel (z) and perpendicular (x) orientations. With momentum $|P_x| < 1$ a.u., the backward rescattering holographic interference pattern in Fig. 1 (c) predicted by SFA agrees with the results by TDSE qualitatively. The shape and the number of the stripes agree. The density of stripes becomes sparse as $|P_z|$ increases. This interference pattern remains with different orientations. With $|P_x| > 1$ a.u., clear interference structure can be found with parallel (z) orientation. The density of the stripes becomes dense as $|P_z|$ increases, and their shape also quantitatively agrees with the SFA model in Fig. 1 (d). We attribute the observation of the weak holography to the Coulomb focusing effect. It is natural that it becomes defocusing effect when the orientation of the molecule is perpendicular. As a result, no clear interference structure appears in Fig. 3 (b) with $|P_x| > 1$ a.u.

The parallel laser-molecule orientation is optimal to identify the backward rescattering holography predicted in Fig. 1 (d). However, the signal is weak in Fig. 3 (a) and perfect

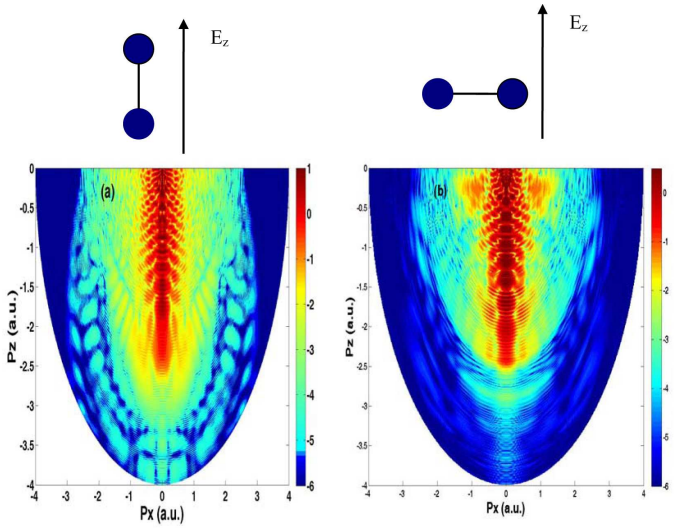

FIG. 3: Photoelectron angular momentum distribution of H_2^+ in a strong laser field of intensity $I = 1.5 \times 10^{15}$ W/cm^2, and wavelength 532 nm. The polarization of the laser field is along the z axis. In (a), the molecular axis is along the z direction. In (b), the molecular axis is along the x axis. The color is plotted on the logarithmic scale. Adapted from Ref. [8], copyright APS

orientation control is generally difficult in experiments. The positive aspect is that the holographic pattern in Fig. 1 (c) is not sensitive to the orientation of the molecules in our simulations. The laser parameters used in our calculations are experimentally accessible currently. Hopefully "backward rescattering" holography may be experimentally developed and confirmed in the future.

Is it possible to observe the four kinds of holography patterns at the same time? To achieve this, we study the photoelectron holography from the asymmetric molecular ion HeH^{2+} [28]. When the laser field polarization is along the molecular z axis, the ionization rate from $+z$ and $-z$ is quite different [29]. The former may be two orders higher than the latter due to enhanced ionization via enhanced excitation [30] and the lower I_p of the H atom. We may therefore neglect the ionization from the $-z$ direction. Consequently, the forward rescattering and the backward rescattering of photoelectron will not overlap, which allows us to study the forward and backward holography simultaneously. The internuclear distance of HeH^{2+} is fixed at $R = 4$ a.u. The laser field is the same as that used for studying H_2^+. The photoelectron angular momentum distribution of HeH^{2+} is illustrated in Fig. 4 with both parallel and perpendicular orientations. For parallel orientation, with $P_z > 0$, the backward rescattering patterns shown in Fig. 1 (c) and (d) from the SFA model, can be clearly identified in Fig. 4. The patterns are similar to the results with H_2^+ presented in Fig. 3. Due to the larger ionization potential and nuclear charge, the interference patterns are distorted, but still distinguishable. For $P_z < 0$, the pattern corresponds to forward rescattering holography. The angular stripes agree with the SFA model illustrated in Fig. 1 (a). The radial rings agree with the SFA model in Fig. 1 (b). The space between

the rings increases as $|P_z|$ increases, agreeing with the SFA model. When we change the laser field polarization direction to be perpendicular to the molecular axis of HeH^{2+}, the momentum distribution of the photoelectrons changes dramatically. This corresponds to forward rescattering holography, similar to the holography patterns shown in Fig. 2. This is attributed to the Coulomb defocusing effect with larger internuclear distance R, where the scattering cross section is relatively small.

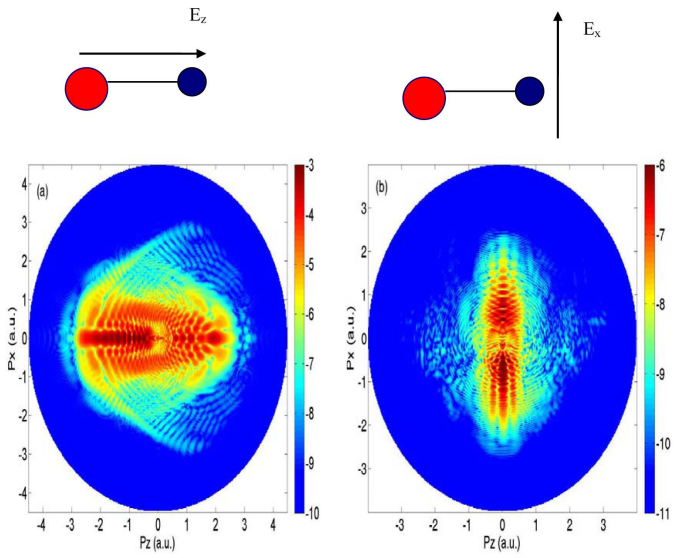

FIG. 4: Photoelectron angular momentum distribution of HeH^{2+} in strong laser field. The laser parameters are the same as in Fig. 3. The molecular axis is along the z direction. In (a), the polarization of the laser field is parallel to the molecular axis. In (b), the molecular axis is perpendicular to the laser polarization. The color is plotted on the logarithmic scale.

V. DISCUSSION AND CONCLUSIONS

In summary, four kinds of photoelectron holography patterns are predicted by an SFA model. These represent subcycle electron dynamics. The first kind of forward rescattering holography has been identified experimentally using low-frequency FELs. The other three kinds of holography patterns are simulated by solving TDSE for symmetric H_2^+ and non-symmetric HeH^{2+} molecular ions in strong short-wavelength lasers. The simulations show that Coulomb focusing effects are crucial for observing backward rescattering interference patterns in ATI. Photoelectron holography encodes rich information on the structure of initial electron states of an electronic system as well as ultrafast processes induced by the laser field. It can provide an attosecond-resolved tool for dynamic imaging of electronic and molecular structure due to subcycle recollision times of ionized electrons. The laser parameters used are accessible experimentally currently due to advances in laser technology.

The present review should stimulate experimental study of photoelectron holography as a new tool in molecular structure research.

Acknowledgements

We thank Y. Huismans, O. Smirnova, K. J. Yuan, and M. J. J. Vrakking for valuable discussions. We thank the RQCHP and Compute Canada for access to massively parallel computer clusters and the CIPI (Canadian Institute for Photonic Innovations) for financial support in its ultrafast science program.

References

[1] D. Gabor, Nature **161**, 777 (1948).
[2] J. J. Barton, Phys. Rev. Lett. **61**, 1356 (1988).
[3] M. Spanner, O. Smirnova, P. B. Corkum, and M. Y. Ivanov, J. Phys. B **37**, L243 (2004).
[4] Y. Huismans *et al.*, Science **331**, 61 (2011).
[5] G. G. Paulus *et al.*, Phys. Rev. Lett. **84**, 3791 (2000).
[6] G. G. Paulus, W. Becker, W. Nicklich, and H. Walther, J. Phys. B **27**, L703 (1994).
[7] X. B. Bian *et al.*, Phys. Rev. A **84**, 043420 (2011).
[8] X.-B. Bian and A. D. Bandrauk, Phys. Rev. Lett. **108**, 263003 (2012).
[9] P. Salières, A. Maquet, S. Haessler, J. Caillat, and R. Taïeb, Rep. Prog. Phys. **75**, 062401 (2012).
[10] T. Zuo, A. D. Bandrauk, and P. B. Corkum, Chem. Phys. Lett. **259**, 313 (1996).
[11] M. Peters *et al.*, Phys. Rev. A **83**, 051403 (2011).
[12] G. Dixit, J. M. Slowik, and R. Santra, Phys. Rev. Lett. **110**, 137403 (2013).
[13] A. D. Bandrauk, S. Chelkowski, and S. Goudreau, J. Mod. Opt. **52**, 411 (2005).
[14] P. B. Corkum, Phys. Rev. Lett. **71**, 1994 (1993).
[15] X. Y. Lai, W. Quan, and X. Liu, Phys. Rev. A **84**, 025401 (2011).
[16] S. Borbély, A. Tóth, K. Tokési, and L. Nagy, Phys. Rev. A **87**, 013405 (2013).
[17] D. G. Arbó, E. Persson, and J. Burgdörfer, Phys. Rev. A **74**, 063407 (2006).
[18] F. Lindner *et al.*, Phys. Rev. Lett. **95**, 040401 (2005).
[19] Y. Huismans *et al.*, Physical Review Letters **109**, 013002 (2012).
[20] T. M. Yan and D. Bauer, Phys. Rev. A **86**, 053403 (2012).
[21] Y. Huismans *et al.*, Phys. Rev. A **87**, 033413 (2013).
[22] D. D. Hickstein *et al.*, Phys. Rev. Lett. **109**, 073004 (2012).
[23] X. M. Tong *et al.*, Phys. Rev. A **88**, 013410 (2013).
[24] M.-H. Xu *et al.*, Phys. Rev. Lett. **107**, 183001 (2011).
[25] P. A. Korneev *et al.*, Phys. Rev. Lett. **108**, 223601 (2012).
[26] T. Marchenko, Y. Huismans, K. J. Schafer, and M. J. J. Vrakking, Phys. Rev. A **84**, 053427 (2011).
[27] T. Brabec, M. Y. Ivanov, and P. B. Corkum, Phys. Rev. A **54**, R2551 (1996).
[28] X.-B. Bian and A. D. Bandrauk, Phys. Rev. A (submitted).
[29] X.-B. Bian and A. D. Bandrauk, Phys. Rev. Lett. **105**, 093903 (2010).
[30] G. L. Kamta and A. D. Bandrauk, Phys. Rev. Lett. **94**, 203003 (2005).